INTERNATIONAL JOURNAL FOR NUMERICAL METHODS IN FLUIDS
Int. J. Numer. Meth. Fluids 2005; **47**:1147–1155
Published online 27 January 2005 in Wiley InterScience (www.interscience.wiley.com). DOI: 10.1002/fld.919

Prediction of jet flows in the supersonic nozzle and diffuser

Yi Liu*,† and Brain J. Bellhouse

Department of Engineering Science, University of Oxford, OX1 3PJ Oxford, U.K.

SUMMARY

The authors' recently-developed code for a needle-free powdered vaccine delivery device, the epidermal powdered inject system (EPI), is summarized in this paper. The behaviour of supersonic jet flows, which accelerate micron sized powdered vaccines to penetrate human skin or mucosal tissue, is therefore of great importance. A well-established modified implicit flux vector splitting (MIFVS) solver for the Navier–Stokes equations is extended to study numerically the transient supersonic jet flows of interest. A low Reynolds number k–ε turbulence model, with the compressibility effect considered, is integrated into MIFVS solver to predict the turbulent structures and interactions with inherent shock systems. The results for the NASA validation case NPARC, Venturi and contoured shock tube (CST) of the EPI system are discussed. Copyright © 2005 John Wiley & Sons, Ltd.

KEY WORDS: supersonic; nozzle; diffuser; Venturi; numerical; powder injection

1. INTRODUCTION

A needle-free device for epidermal delivery of powdered vaccines and/or drugs has been reported [1]. This epidermal powdered injection system (EPI) uses a transient supersonic jet to accelerate micron sized vaccines (in general sense, any particle in micro-form) to a velocity sufficient to penetrate the outer layer of human skin or mucosal tissue. The performance of the EPI system depends on controlling both particle velocity and distribution. The behaviour of the supersonic or sonic jet issuing from a converging–diverging nozzle or a diffuser throat is therefore of great importance.

The objective of the present study is to perform numerical investigations of supersonic jet flows by extending a well established modified implicit flux vector splitting steady solver (MIFVS) to a transient solver, integrated with a compressible low Reynolds number k–ε

*Correspondence to: Yi Liu, Department of Engineering Science, University of Oxford, Parks Road, OX1 3PJ Oxford, U.K.
†E-mail: yi.liu@eng.ox.ac.uk

Contract/grant sponsor: PowderJect Plc
Contract/grant sponsor: Chiron Vaccines Inc

Received 27 April 2004
Revised 15 December 2004
Accepted 16 December 2004

turbulence model. An important consideration in the development of the MIFVS has been the establishment of an implicit difference scheme and eigenvalue analysis of the matrix for the Navier–Stokes equations [2, 3].

This paper is organized as follows: Section 2 highlights the main features of the numerical methods employed for the transient MIFVS solver. This numerical approach is first calibrated in Section 3 by qualitative comparisons with the NASA validation case, NPARC. In Section 4, new insights into the EPI delivery system will be extensively explored through presenting and analysing the results obtained for two different EPI devices, one using a Venturi effect to draw particles into the gas stream (Venturi), the other based on a shock tube design, referred to as a contoured shock tube (CST). Finally, we draw some conclusions.

2. NUMERICAL METHOD

2.1. Governing equations

The Reynolds averaged Navier–Stokes equations (RANS) for an axisymmetric flow are written in a conservative flux-vector-splitting form and in generalized co-ordinates [2], with the source terms of $\hat{S}_1$ and $\hat{S}_2$ originating from cylindrical co-ordinates, as

$$\frac{\partial \hat{U}}{\partial t} + \frac{\partial \hat{F}_i^+}{\partial \xi_i} + \frac{\partial \hat{F}_i^-}{\partial \xi_i} + \hat{S}_1 = \frac{1}{Re}\left[\frac{\partial \widehat{F_{vi}}}{\partial \xi_i} + \hat{S}_2\right] \tag{1}$$

2.2. Implicit formulation

An implicit formulation of the RANS equations has been developed over the past few years, which uses the spectral radii technique to simplify the calculation and at the same time avoids the approximate-factorization (AF) to increase the time step and stability [2].

Implicit formulation for Equation (1) is constructed, in the semidiscrete delta form, as

$$\begin{aligned}\frac{\partial(\delta\hat{U}^{n+1})}{\partial t} = \frac{\Delta\hat{U}^n}{\Delta t} + \Bigg[& -\sum_{i=1}^{2} \frac{\partial(\lambda_i^+ \delta\hat{U}^{n+1} + \lambda_i^- \delta\hat{U}^{n+1})}{\partial \xi_i} \\ & -\lambda_{1s}\delta U^{n+1} + \sum_{i=1}^{2} \frac{\partial(\lambda_{vi}\delta\hat{U}^{n+1})}{\partial \xi_i} + \sum_{i=1}^{2} \frac{\partial(\lambda_{2s}\delta\hat{U}^{n+1})}{\partial \xi_i}\Bigg] \\ \hat{U}^{n+1} = \hat{U}^n + \delta\hat{U}^n & \end{aligned} \tag{2}$$

where $\lambda_i^{\pm}$, λ_{vi}, λ_{1s} and λ_{2s} are the spectral radii of Jacobians of the convection, dissipation and source terms. $\Delta\hat{U}^n$ is evaluated in the explicit step through flux vector splitting (FVS)

$$\Delta\hat{U}^n = \Delta t\left[-\sum_{i=1}^{2} \frac{\Delta_- \hat{F}_i^+}{\Delta\xi_i} - \sum_{i=1}^{2} \frac{\Delta_+ \hat{F}_i^-}{\Delta\xi_i} - \hat{S}_1 + \frac{1}{Re}\left(\frac{\Delta_c \hat{F}_{vi}}{\Delta\xi_i} + \hat{S}_2\right)\right]^n$$

where $(\Delta_-(\bullet))/\Delta\xi_i$, $(\Delta_+(\bullet))/\Delta\xi_i$ and $(\Delta_c(\bullet))/\Delta\xi_i$ denote backward, forward and central difference, respectively.

It has been demonstrated that the present implicit formulation is adequately efficient when FVS is employed, while maintaining a high level of robustness and accuracy. The multigrid

strategy, in conjunction with a local time step, is implemented to further accelerate convergence in the MIFVS solver [2, 3].

2.3. Turbulence model

In this study, a low Reynolds number k–ε model proposed by Chien [4], with Sarkar's compressibility modification [5], is implemented into the MIFVS code to simulate the turbulence boundary layer and its interaction with shock waves.

The mathematical equation for the low Reynolds number k–ε model is reformulated into the same form as Equation (1). Therefore, it is pretty straightforward to extend the methods of implicit formulation and eigenvalue analysis of RANS equations.

2.4. Transient calculation

The MIFVS has proven to be very efficient for many steady problems [2, 3]. However, this time-dependent solver is no longer accurate for transient calculations. Dual time stepping is thus carried out to provide an efficient time-dependent solution of unsteady flows.

By introducing a pseudo time (or fictitious time) τ, the governing equations can be reformulated as

$$\frac{\partial \hat{U}}{\partial \tau} = \frac{\partial \hat{U}}{\partial t} + R(\hat{U}) = R^*(\hat{U}) \tag{3}$$

where t is a physical time (or real time), and $R^*(\hat{U})$ denotes a pseudo residual while marching in the pseudo time, τ. The real time residual, $R(\hat{U})$, can be derived from Equation (1).

2.5. Multiblock structure and computational grid

In order to generate a better quality grid for different zones of interest, multi-block topology is employed. In each zone, a specific distribution, a smooth combination of linear and logarithmic functions across the nozzle radial direction, is accomplished to refine the mesh near a wall to ensure the boundary layer resolution.

The results presented in this paper have been verified to ensure grid-independent solutions.

3. VALIDATION

The NASA validation case, NPARC, which involves a 'submerged' turbulent supersonic jet emanating from an axisymmetric converging–diverging Mach 2.22 nozzle [6], is firstly calculated using the MIFVS method.

Figure 1 plots Mach number contours. A very similar flow field pattern is shown in the literature [6]. A turbulent shear layer develops downstream from the nozzle lip, and grows linearly as the jet entrains fluids from the surrounding medium. The shear layer reaches the jet axis between $25R$ and $26R$ (R is the radius of the nozzle exitplane) downstream of the nozzle exit, enclosing a region of Mach 2.2 flow. Note that Mach number contours near the nozzle exit show the occurrence of periodic vortex shedding even in the current steady nature of the calculation. In detail, the representative velocity profile is plotted in Figure 2, at the position where $x/R = 73.80$ downstream of the nozzle exit. Here, prediction by the present

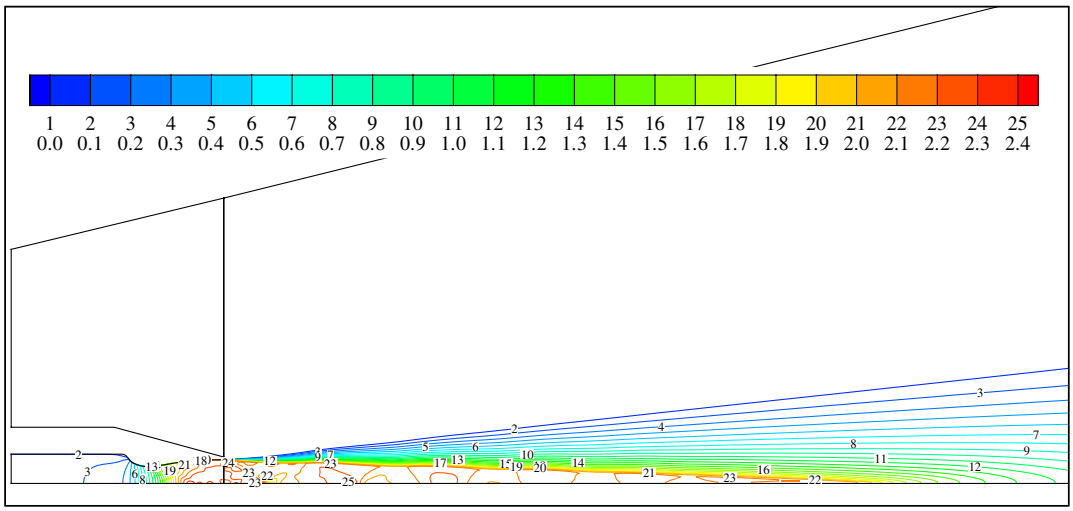

Figure 1. Contour plot of Mach number.

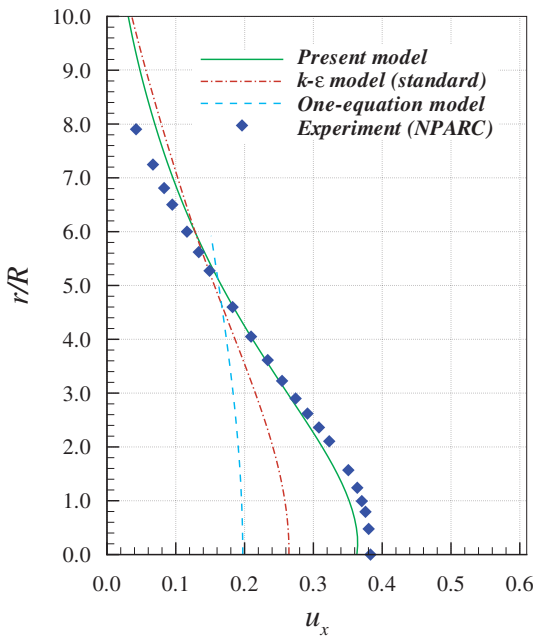

Figure 2. Velocity profiles.

method is compared with the result obtained from the MIFVS solver with the standard k–ε model and with experimental measurements. The simulated velocity distribution, using the Spalart–Allmaras one-equation model by NPARC [6], is also plotted. In all the comparisons, the present MIFVS solver with the modified k–ε turbulence model gives the best agreement.

This code is then applied to prototypes of the EPI system based on the Venturi principle (Venturi [7]) and a contoured shock tube (CST [8, 9]), respectively.

4. RESULTS AND DISCUSSION

4.1. Venturi powder injection system

One form of the EPI system, called a Venturi device (Venturi, Figure 3), utilizes the Venturi effect to entrain powders. The Venturi device has been developed and intensively investigated experimentally and analytically [7]. MIFVS calculations are performed here in an attempt to gain some insights into the flow characteristics of the Venturi system, to provide some fundamental understanding and optimize the aerodynamic design.

We simulate two typical operating conditions for the Venturi device, nominally 35 and 25bar for the upstream total pressure. The conditions of interest represent the upper and lower bounds of the particle delivery window. The calculated Mach number profiles are compared with experimental measurements in Figure 4. The experimental data were obtained from Pitot probe and nearby static pressure transducer measurements (shown in Figure 3) by using the Rayleigh Pitot tube formula. Generally, the exit Mach number distribution is in good agreement with measurements for the lower (25 bar) condition. However, the asymmetric distribution for the higher (35 bar) condition is not observed due to the nature of the axisymmetric solver. The complexity of interactions between shock waves, the turbulent boundary layer and the free shear layer, can be best appreciated in velocity magnitude contours, Figure 5.

The calculations lead to a closer examination of unsteadiness near the separated jets. The calculation turns transient when the solution reaches convergence. The quasi-periodic phenomenon, due to the overexpanded nozzle condition, is illustrated in Figure 6. Figure 7 corresponding power spectra obtained by FFT analysis for the pressure history over

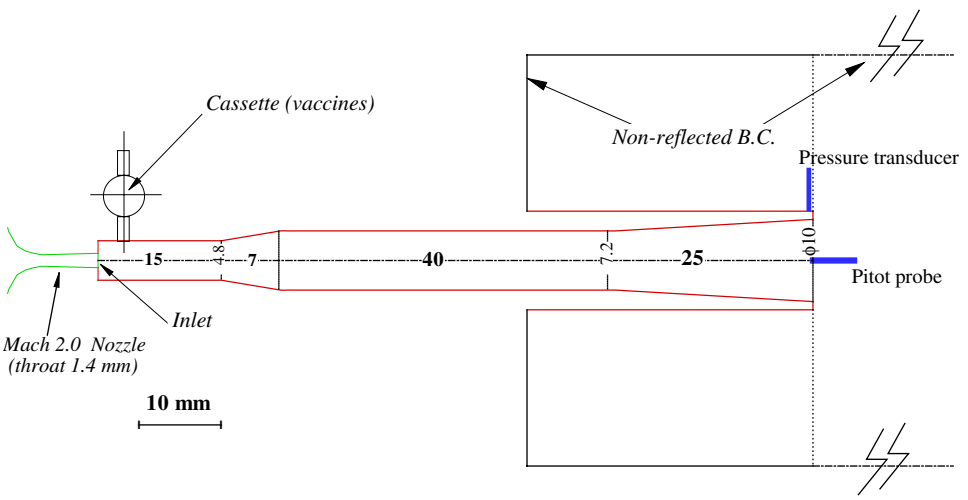

Figure 3. Configuration of prototype Venturi.

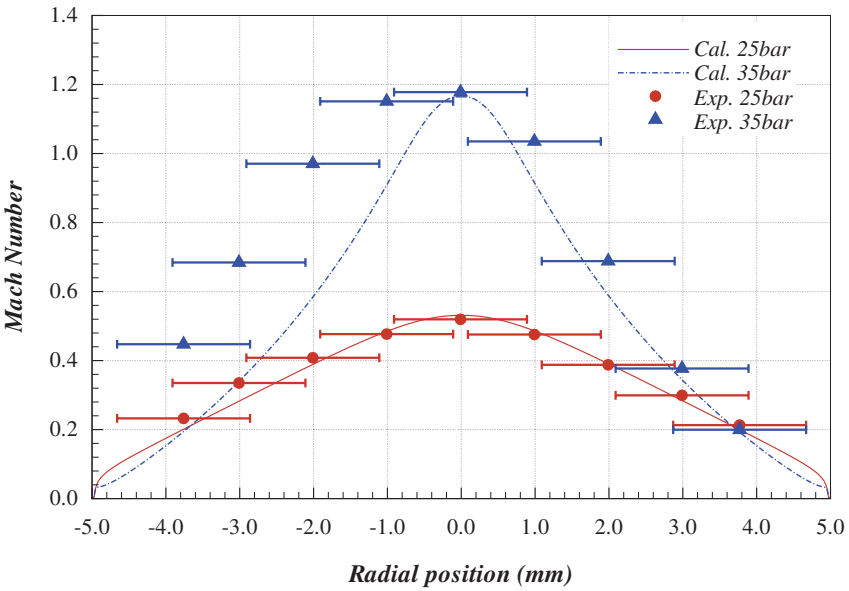

Figure 4. Mach number along Venturi exit.

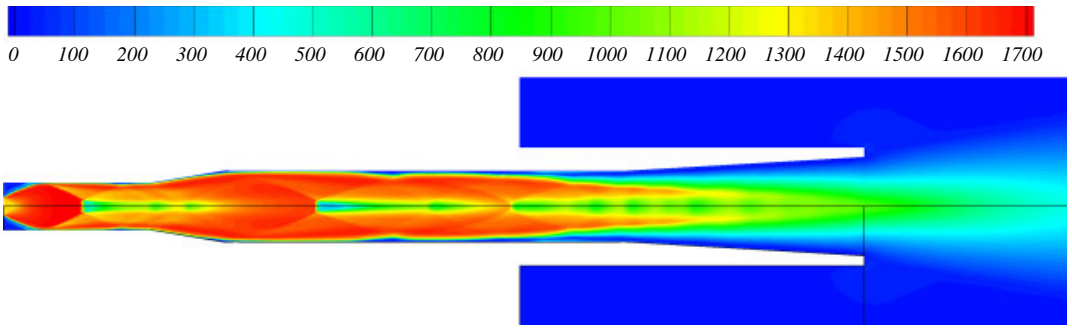

Figure 5. Calculated contour plots of velocity magnitude.

shows the 100 periods. The dominant frequency of $1.69e+5$ Hz is found. The corresponding Strouhal number, based on the inlet diameter and jet velocity of Venturi device, is equal to 0.222.

4.2. *Contoured shock tube system*

The CST device uses a particle cassette (consisting of a rigid cylinder, capped top and bottom with a polymeric membrane) to hold the vaccine particles. When the driver helium gas is released, both membranes of the cassette rupture and the vaccine particles are entrained in the transient shock tube flow. The shock tube is gradually increased in diameter in its downstream portion, hence the term 'Contoured Shock Tube' [8, 9]. One variant of the CST system is shown in Figure 8.

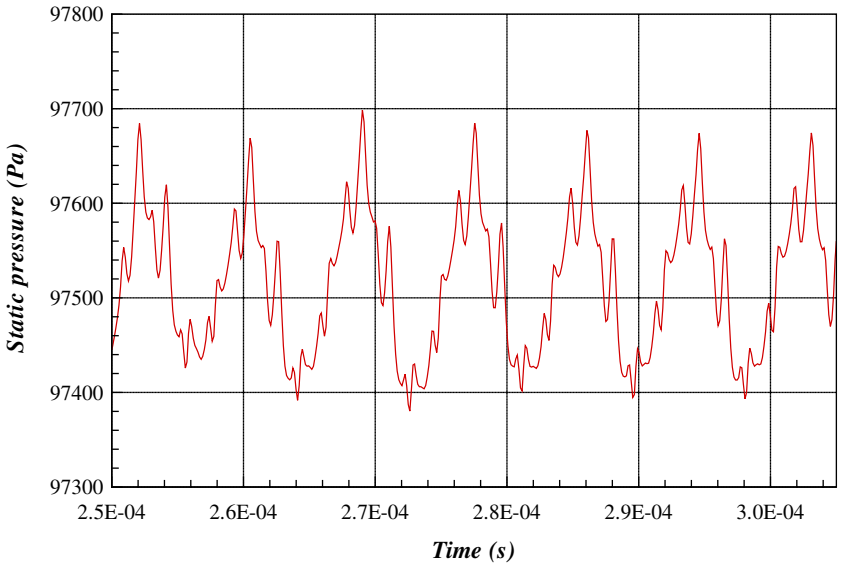

Figure 6. Variation of instantaneous pressure.

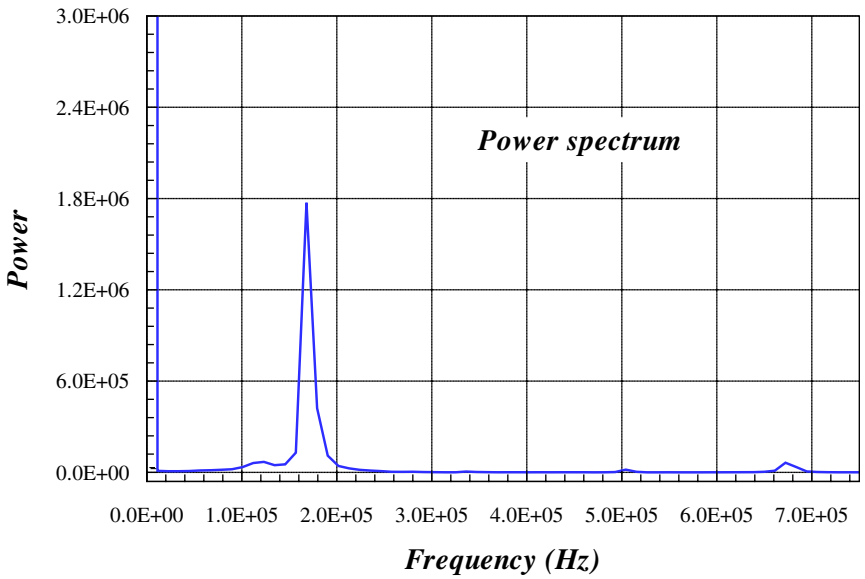

Figure 7. Spectrum of pressure recorded in Figure 6.

Figure 9 presents variations of Mach number with time at the CST exit. The Mach number profile calculated using a commercial software, *Fluent* (Fluent Inc., U.S.A.), is plotted for comparison. Figure 9 illustrates a typical nozzle starting process. The flow is initiated

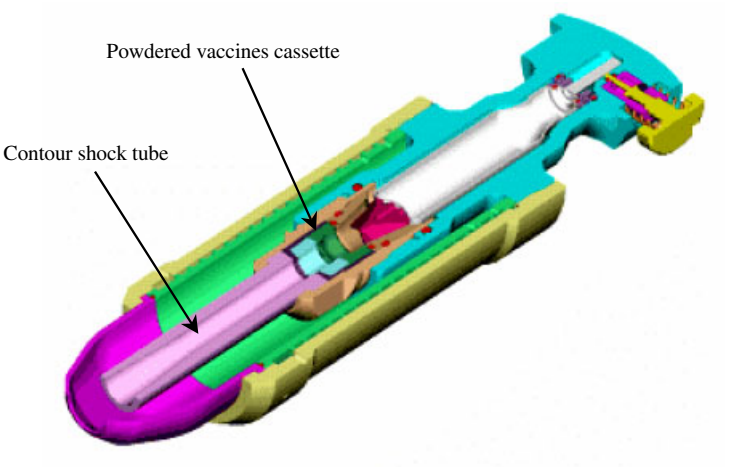

Figure 8. A schematic of CST device.

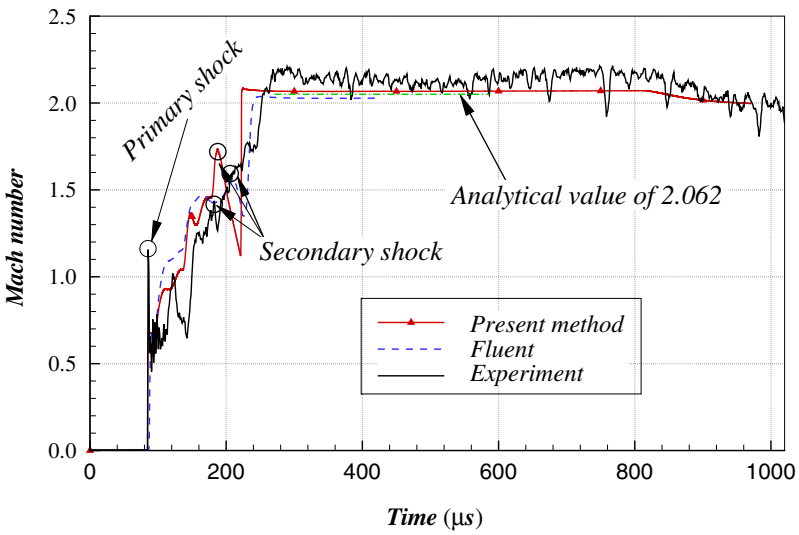

Figure 9. Mach number histories at the CST exit.

by a primary shock (indicated by a sudden Mach number rise), which opens a transient starting process, followed by a contact surface and a secondary shock wave, finally reaching a quasi-steady supersonic flow region (QSSF). The Mach number of the QSSF predicted by the present approach is 2.067, compared with the analytical derived value, 2.062, and experimental measurement, $2.14^{\pm 0.4}$ ($\text{Mean}^{\pm \text{Standard deviation}}$). Meanwhile, a slightly lower level, 2.027, is calculated by virtue of the *Fluent* code. In general, the starting process is well modelled in terms of shock strength, termination time and the QSSF level.

5. CONCLUSIONS

An efficient numerical solver, MIFVS, has been extended to solve the transient supersonic jet flows generated for epidermal delivery of powdered vaccines. A low Reynolds number k–ε turbulence model, with the compressibility effect considered, has been implemented and demonstrated to be numerically stable, accurate and efficient for solving the supersonic jet flows through extensive comparisons with the NASA validation case, NPARC, and prototypes of the EPI delivery system. Results obtained show good agreements with experimental data and other published numerical results, the main flow features being well predicted.

ACKNOWLEDGEMENTS

The authors wish to acknowledge PowderJect Plc. and Chiron Vaccines Inc. for their financial support. Dr Costigan and Dr Kendall are thanked for providing experimental data of the prototype EPI system.

REFERENCES

1. Bellhouse BJ, Sarphie DF, Greenford JC. Needless syringe using supersonic gas flow for particle delivery. *International Patent WO94/24263*, 1994.
2. Liu Y. Numerical method of three-dimensional viscous flow in turbomachinery multistage environment. *Ph.D. Thesis*, Xi'an Jiaotong University, China, 1996.
3. Liu Y, Kendall MAF, Bellhouse BJ. An efficient implicit finite difference scheme for transonic flow. *Proceedings of the 32nd AIAA Fluid Dynamics Conference*, *AIAA 2002-2955*, St. Louis, MO, USA, 2002.
4. Chien KY. Predictions of channel and boundary layer flows with lower-Reynolds-number turbulence model. *AIAA Journal* 1982; **20**(1).
5. Sarkar S, Erlebacher G, Hussaini MY, Kreiss HO. The analysis and modelling of dilational terms in compressible turbulence. *Journal of Fluid Mechanics* 1991; **227**:473–493.
6. Eggers JM. Velocity profiles and eddy viscosity distributions downstream of a Mach 2.22 nozzle exhausting to quiescent air. *NASA TN D-3601*, 1966.
7. Costigan G, Liu Y, Brown GL, Carter FV, Bellhouse BJ. Evolution of the design of Venturi devices for the delivery of dry particles to skin or mucosal tissue. *Proceedings of the 24th International Symposium on Shock Waves*, Beijing, China, 2004.
8. Kendall MAF. The delivery of particles vaccines and drugs to human skin with a practical, hand-held shock tube-based system. *Shock Waves Journal* 2002; **12**(1).
9. Liu Y, Kendall MAF, Truong NK, Bellhouse BJ. Numerical and experimental analysis of a high speed needle-free powdered vaccines delivery device. *Proceedings of the 20th AIAA Applied Aerodynamics Conference*, *AIAA 2002-2807*, St. Louis, MO, USA, 2002.

